Experimental and numerical investigation on frame structure composed of steel reinforced concrete beam and angle-steel concrete column under dynamic loading

K. Wang[1], S.F. Yuan[2],*, D.F. Cao[3], W.Z. Zheng[4]

Abstract

This paper describes experimental and numerical investigations on two specimens of frames composed of steel reinforced concrete beam and angle-steel concrete column under horizontal low cyclic loading. Based on the test results, the relationship curves of the horizontal load-displacement and the failure modes are acquired. Meanwhile the hysteretic behaviors, skeleton curves, stiffness degradation, energy dissipation, residential deformation of the two specimens are studied. Nonlinear structural analysis program OpenSEES is employed to predict the experimental curves. Using the verified numerical model, the influences of slenderness ratio, axial compression ratio, steel ratio of column, cross-section moment resistance of I-shaped steel in beam, ratio of longitudinal rebars of beam and prestressing level on skeleton curves are investigated. The results indicated that the two specimens exhibited the favorable ductility and energy dissipation capacity, and the beam depth could be reduced to improve service function because of the application of the prestress. The ultimate horizontal load decreases with the increase of column slenderness ratio, and firstly increases then decreases with the increase of axial compression ratio. In the meantime, the descent segment of skeleton curve is smooth with the increase of column slenderness ratio, and becomes steeper with the increase of axial compression ratio.

1. Introduction

Adding storeys for an existing building using separated out-jacketing frame structure without connecting to the foundation and superstructure of the original structure is a traditional technique in China [1, 2]. The existing building could be built of any type of structure, such as concrete, steel, masonry and even composite structure. Based on the idea of self-weight-carried floor under construction proposed by Zheng et al. [3], a new type of separated out-jacketing frame structure composed of steel reinforced concrete beam and angle-steel concrete column (SRCB-ASCC Frame) is proposed in this paper, as shown in Fig. 1. When the vertical load is too big, the steel reinforced concrete beam could be prestressed to decrease the beam crack width and vertical deformation. In order to avoid the slip failure between encased steel beam and concrete, the

steel beam is welded with steel anchors in the panel zone, and the length of steel anchor could be calculated to prevent punching failure according to the reference [4].

This new type of frame structure has an advantage over the conventional one as the steel beam could carry the own weight of the frame beam and the construction loads when the frame is under construction, and then the steel reinforced concrete beam and the angle-steel concrete column could work as a unit to carry remainder loads after the concrete is cured.

In order to obtain the dynamic performance of SRCB-ASCC Frame, nine angle-steel concrete column specimens with the shear-span ratio of 3.0, axial compression ratio of 0.33~0.42, and the steel plate stirrup ratio of 1.18%~2.09%, were tested under horizontal low cyclic loading, and the M-φ hysteretic model was established by Zheng and Ji [5,6]. Four prestressed and unprestressed steel reinforced concrete beams were also experimental investigated under vertical low cyclic loading by Xue et al. [7], and seven prestressed steel reinforced beams with different designing coefficients were tested under static loading by Zhao et al. [8]. Furthermore, two frames of one-story and one-bay with solid-web steel reinforced concrete members were studied by Fu et al. [9], and related valued datum were acquired.

Although the related members and frames were studied by previous work and references, many problems of the

* Corresponding author: wangkun@yzu.edu.cn

1 phD Lecturer - College of Civil Science and Engineering, Yangzhou Univercity
2 Bachelor Postgraduate Student - College of Civil Science and Engineering, Yangzhou Univercity
3 phD Professor, College of Civil Science and Engineering, Yangzhou Univercity
4 phD Professor, School of Civil Engineering, Harbin Institute of Technology

SRCB-ASCC Frame are still existing: firstly, the seismic performance of the frame as a whole with steel reinforced concrete beam and steel-angle concrete column is rarely tested; secondly, the ground floor columns of the frame are taller than ordinary one, and the seismic performance could be effected by the slenderness of columns and the ratio of beam span to storey height of the ground floor; thirdly, the influence of the encased steel skeleton of the concrete columns on the distribution and development of cracks under earthquake action is also unreported. Thus, this paper conducted an experimental and numerical investigation on the seismic performance of two specimens of SRCB-ASCC Frame under horizontal low cyclic loading to explore the availability in seismic area for further application.
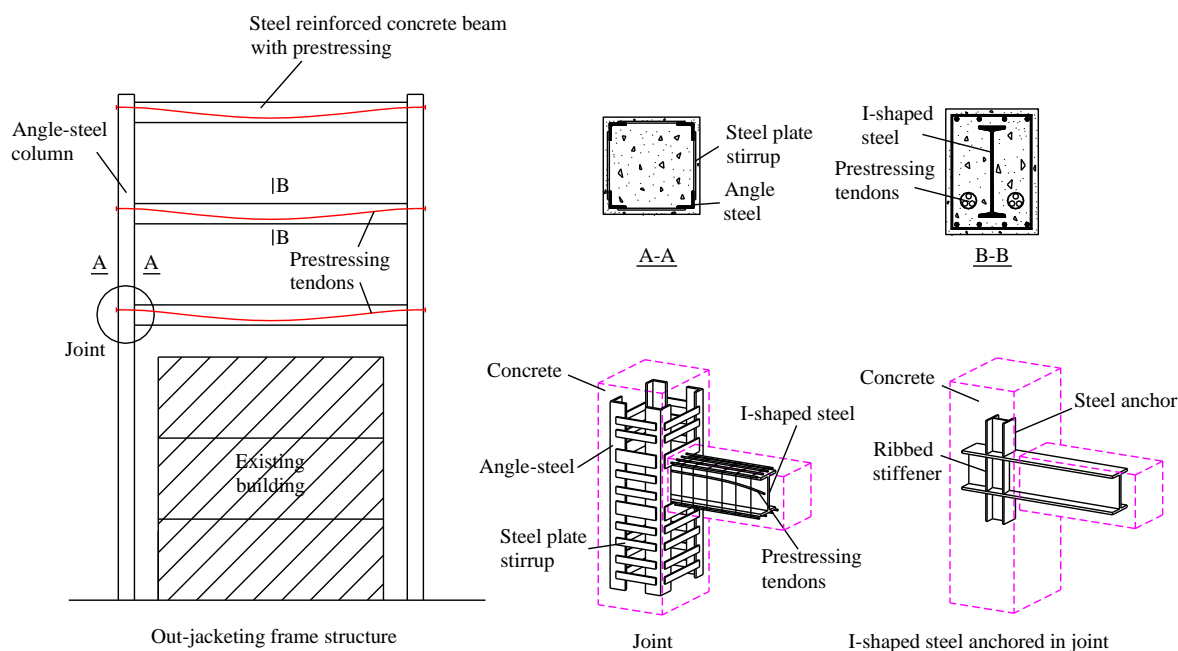
Fig. 1 Schematic view of out-jacketing frame and beam-column connection

2. Experiment

2.1. Specimens design and loading apparatus

A Schematic view of two specimens of SRCB-ASCC Frame was shown in Figure 2. All the specimens have the same shear-span ratio of 5.0 and the axial compression ratio of 0.1, and the requirements of strong-column-weak-beam and strong-joint-weak-member were ensured. One of the specimens was prestressed by using bonded post-tensioned technique, and the prestressing tendons with curvilinear distribution was adopted as Grade 1760 ofφ5. The concrete of the specimens were constructed in two stages, fist from the bottom to the height of 2.5m and then the rest. In order to prevent the slip failure between the encased I-shaped steel and concrete in the panel zone, the connection of the beam to column was designed with the approach of welding steel anchors on the top and bottom of the I-shaped steel flange, and the extended length is

200mm and 350mm respectively. In the specimens design, in order to prevent the longitudinal rebars from passing through the angle steel, the rebars were placed on the top and bottom of the I-shaped steel flange, thus the rebars should pass through the welded steel anchors, and so that the welded steel anchors were strengthened by the C-shaped stiffening ribs, as shown in 5-5 and 6-6 of Figure 2(a) and 2(b). Figure 3 and 4 give the distribution of the prestressing tendons and the shape of two specimens, respectively.

The prestressing tendons are tensioned with the control stress of 1252N/mm^2 at one beam end, and the effective prestressing stress σ_{pe} is 1199N/mm^2 by measuring the average strain of the strain gauges affixed to the tendons near the opposite beam end.

Table 1 lists the mechanical properties of steel of Grade Q235, the rebars of Grade HRB335 and the stirrups of Grade HPB235. Table 2 and table 3 give the mechanical properties of prestressing tendons and concrete respectively.
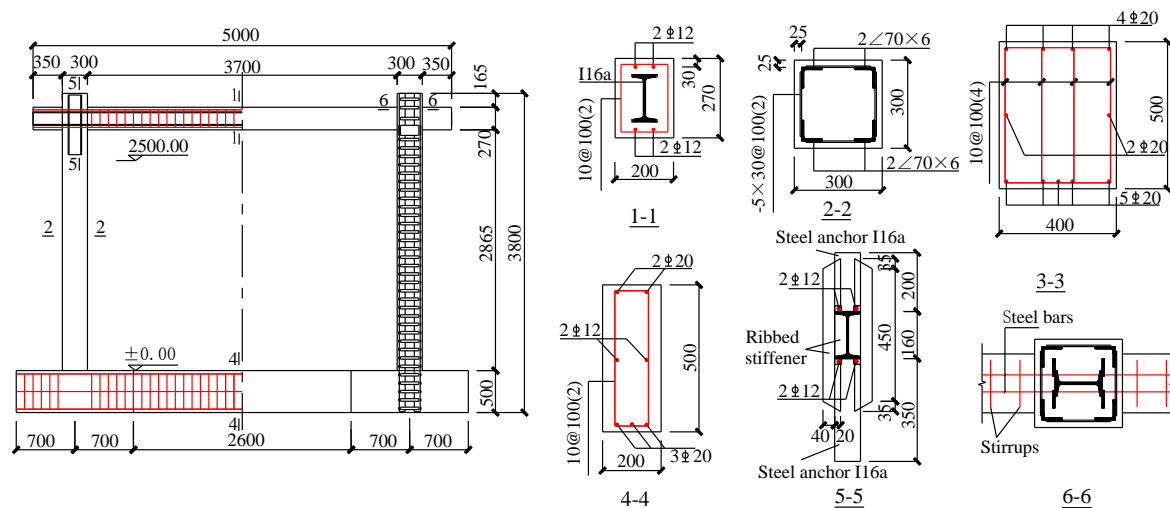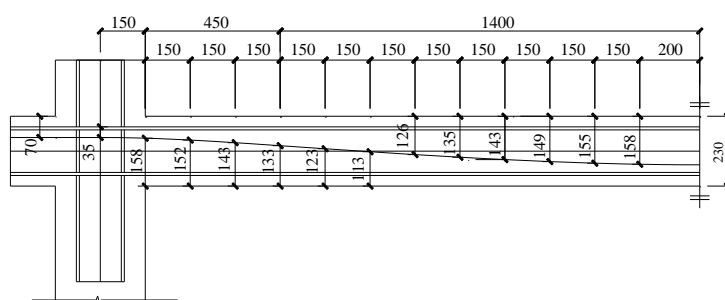
(a) Reinforcements of SRCF
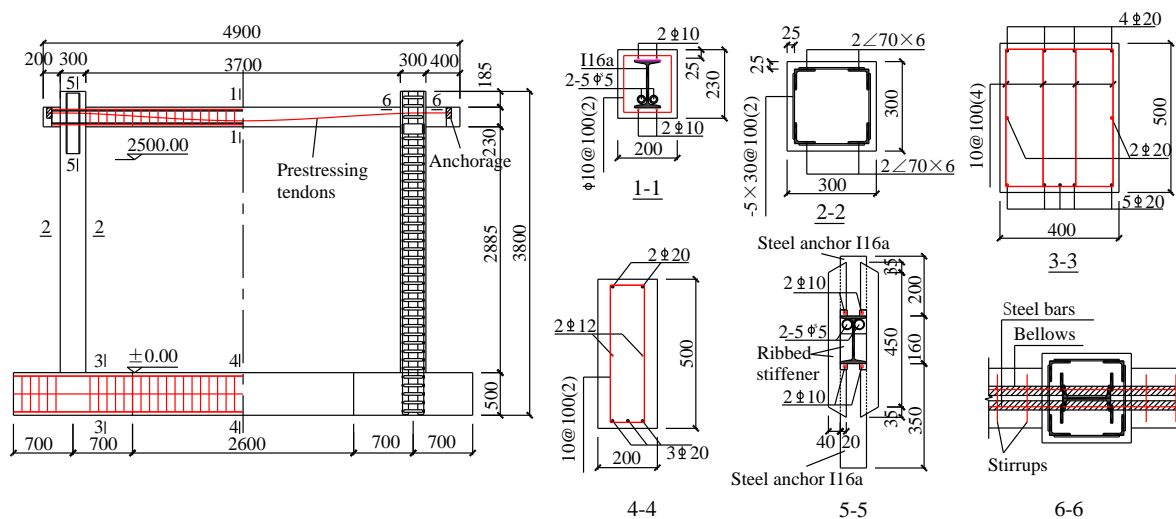
(b) Reinforcements of PSRCF
Fig. 2 Reinforcements of two specimens (units: mm)

Fig. 3 Distribution of the prestressing tendons (units: mm)

Fig. 4 Specimens of two frames

Table 1 Mechanical properties of steel

Specification	Yield strength f_y /N·mm^{-2}	Ultimate strength f_u /N·mm^{-2}	Elastic modulus E_s /N·mm^{-2}
I16a	302.3	450.3	2.0×10^5
∠70×6	287.0	424.3	2.0×10^5
-5	312.0	446.3	2.0×10^5
⏀10	348.7	522.7	2.0×10^5
⏀12	338.6	494.0	2.0×10^5
⏀10	303.0	445.0	2.0×10^5

**Table 2** Mechanical properties of prestressing tendons

| Diameter D/mm	Failure strength f_u / N·mm^{-2}	Nominal yield strength $f_{0.2}$ / N·mm^{-2}	Elongation / %	Sectional shrinkage rate / %	Elastic modulus E_s/ N·mm^2
5.0	1686	1470	5	3.9	2.0×10^5

Table 3 Mechanical properties of concrete

Specimens	Members	Average cubic specimen (100 mm×100 mm×100 mm) compressive strength	Average prismatic specimen (150mm×150mm×300mm) axial compressive strength (MPa)	Elastic modulus E_c / N·mm^{-2}
SRCF	Column	47.9	30.4	3.42×10^4
	Beam and joint	69.8	44.3	3.70×10^4
PSRCF	Column	45.6	29.0	3.38×10^4
	Beam and joint	71.1	45.2	3.72×10^4

Figure 5 and 6 shows the test setup. As show in these pictures, the low cyclic horizontal loading P was applied along the axis of the beam, and the frame was fixed on the ground. The vertical concentrated loads with the 30% value of 400kN and 30kN were applied on the top of the columns and along the beam at the beginning of the tests for pre-loading, and then the full loads were applied and kept constant. The load-displacement hybrid control rules were adopted in the test, and the load and the displacement control method are applied before and after the specimens yield, respectively, as shown in Figure 7. The rightward loading is regarded as the forward direction.
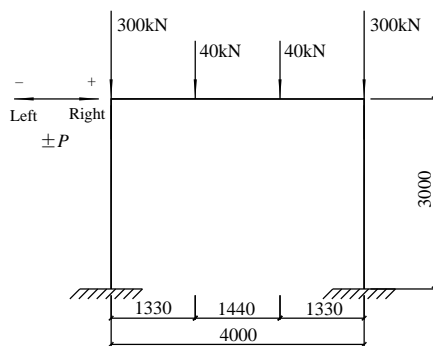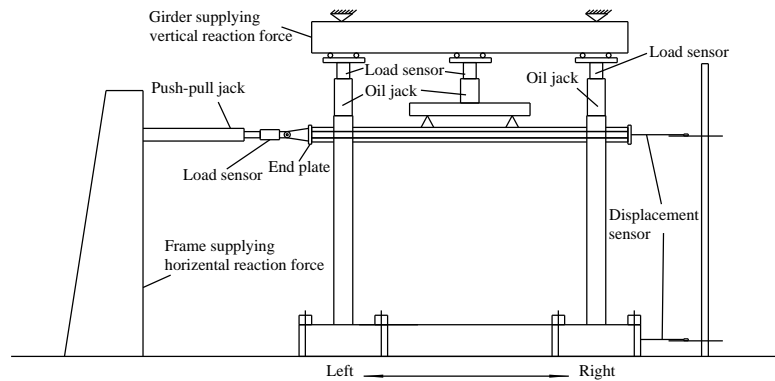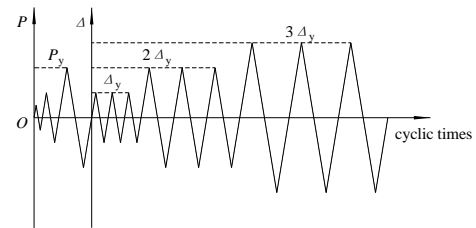

(a) Sketch of loading   (b) Loading apparatus

Fig. 5 Loading and loading apparatus of specimens
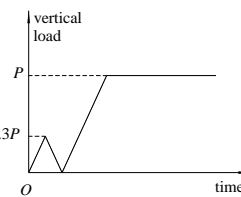
(a) Vertical loading   (b) Horizontal loading

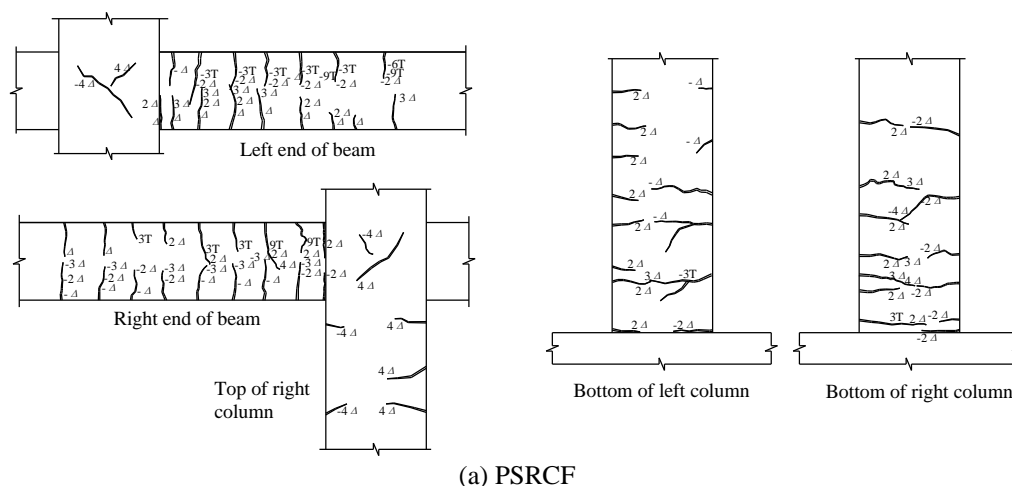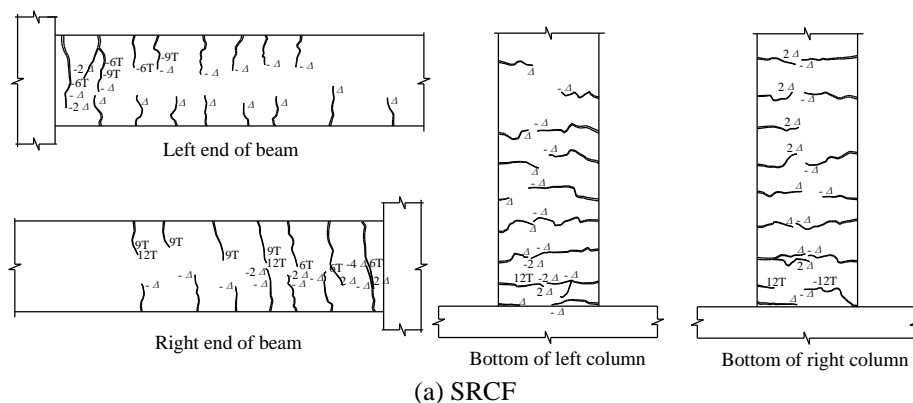**Fig. 6** Loading in tests   **Fig. 7** Loading rule in tests
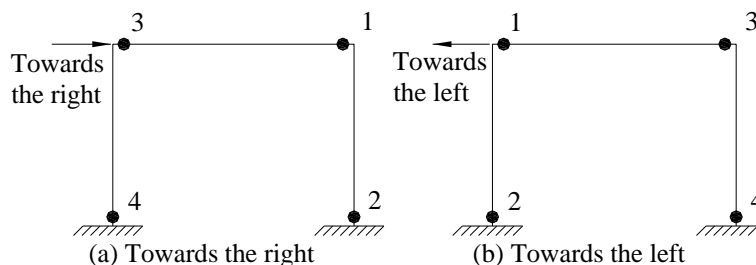
2.2. Cracks and plastic hinges

Figure 8 gives the crack distribution on the beams, columns and joints of the two test specimens. The sequence of the plastic hinges occurring shown in Figure 9 is acquired by measure the value of strain gauges affixed to the steel web and angle-steel, according to the assumption that yielding of cross-sectional I-shaped steel flange and tensile angle-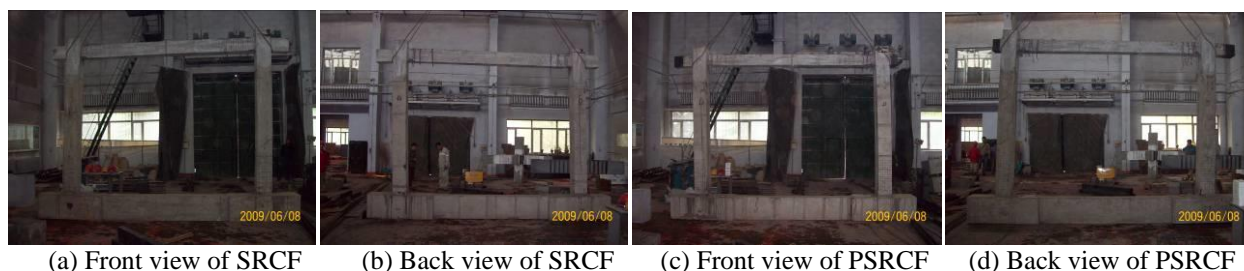steel is recognized as yielding of beam and column respectively. It reveals that plastic hinges of two specimens occurred in the beams and columns by turns rather than firstly in the beams and subsequently in the columns due to the reason that columns of the specimens were so high that the bottom of the column acquired considerable bending moment under the horizontal loading. Figure 10 shows the failure mode of two specimens, and it is found that the concrete of the beam ends suffered more damage than that of the column bottoms.

K. Wang, S.F. Yuan, D.F. Cao, W.Z. Zheng

Left end of beam

Right end of beam

Bottom of left column

Bottom of right column

(a) SRCF

Left end of beam

Right end of beam

Top of right column

Bottom of left column

Bottom of right column

(a) PSRCF

Fig. 8 Distribution of cracks of two specimens

Towards the right

Towards the left

(a) Towards the right

(b) Towards the left

Fig. 9 Sequence of plastic hinges occurring in two specimens

(a) Front view of SRCF   (b) Back view of SRCF   (c) Front view of PSRCF   (d) Back view of PSRCF

Fig. 10 Failure modes of two specimens

2.3. Hysteretic and skeleton curves

Hysteretic curves of two specimens are shown in Figure 11 (a) and (b) respectively, and Figure 12 shows the skeleton curves. From these curves, the following characteristics could be obtained:

(1) The P-Δ curves evidently show the elastic properties with neglectable residual deformation at the initial stage of loading and unloading. As the load increases, the P-Δ curves bend gradually with a certain amount of residual deformation resulted during unloading. When the skeleton curves undergone the nonlinear stage, both of the loading and unloading stiffness reduce gradually, and the reduction increases with the cyclic times.

(2) The hysteretic loops are relatively plump with a spindle shape. After the horizontal load reaches the maximum value, the hysteretic curves under different circles at the same displacement are closer to each other.

(3) The lateral stiffness and hysteretic curves of the two specimens are so similar that prestressing could reduce the height of the beam without decreasing the seismic performance.
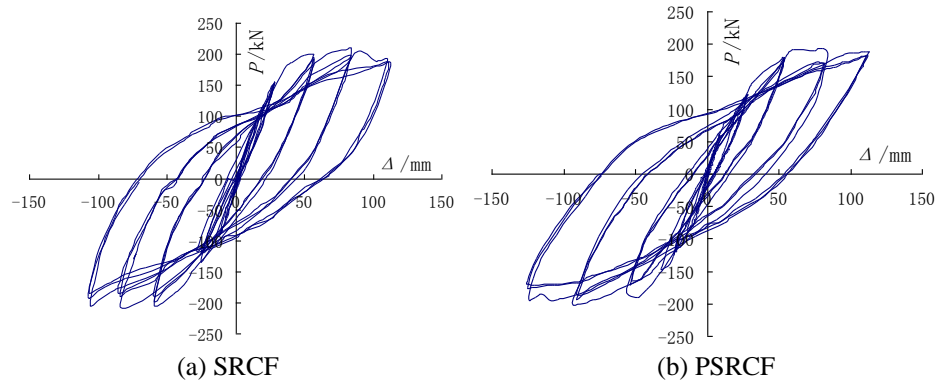

(a) SRCF　　　　(b) PSRCF

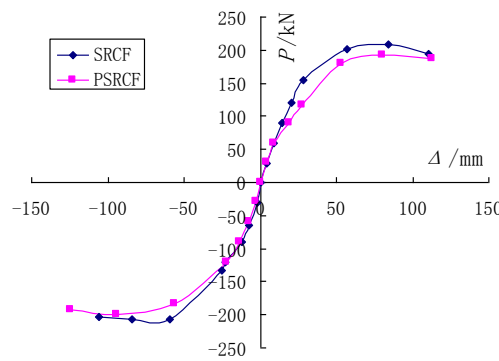**Fig. 11** Hysteretic curves of two specimens

Fig. 12 Skeleton curves for two frames

2.4. Energy dissipation

Figure 13 gives the comparison between energy dissipation of the two test specimens. It demonstrates that energy dissipation coefficient E increases with the displacement Δ increasing. The energy dissipation of two specimens are similar as well as small when the displacements are at the initial stage, while the energy dissipation capacities of the nonprestressed specimens are higher than the prestressed one with the increasing of displacements.
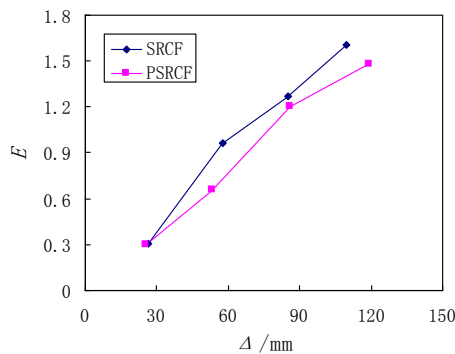
2.5. Stiffness degradation

Figure 14 shows the relationship between secant stiffness coefficient K and displacement Δ. A conclusion is arrived that the secant stiffness of two specimens reduces gradually with the increase of displacement and the stiffness degradation curves are closed to each other.
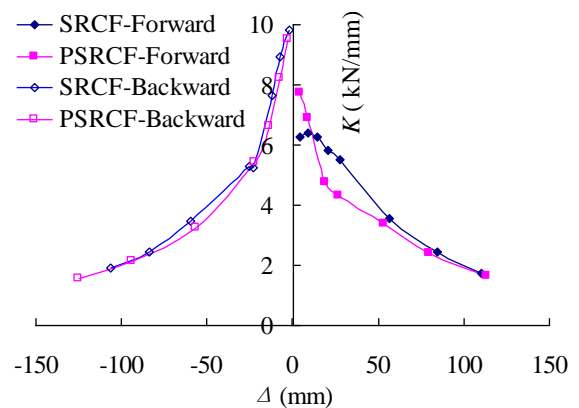

Fig. 13 Energy dissipation coefficients E versus displacement

Fig. 14 Secant stiffness coefficients K versus displacement

K. Wang, S.F. Yuan, D.F. Cao, W.Z. Zheng

2.6 Deformation restoring capacities

Figure 15 gives the residual deformation rate (Δ_0/Δ_u) of two specimens which experienced the maximum horizontal displacement at the unloading point, where Δ_u and Δ_0 is the experienced maximum horizontal displacement and the residual deformation after unloading respectively. It is found that prestressed test specimen has better deformation restoring capacities since its residual deformation is less than that of the nonprestressed one except for $\Delta \approx 27mm$.
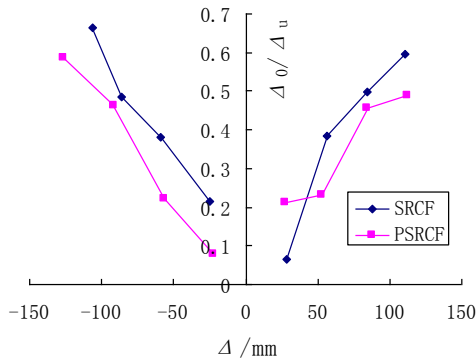

Fig. 15 ratio of residential deformation versus displacement

3. Hysteretic Behavior Analyses

Although in primary studies, the sophisticated FEA model was developed to gain the mechanism behavior of this new type of frame structure [10], the hysteretic behavior and relative factors are still needed to investigate the seismic performance.

OpenSEES as a nonlinear structural analysis program

is made use of to predict the hysteretic curves of two specimens under horizontal low cyclic loading [11]. The basic assumptions for OpenSEES modeling are given: (1) a plane cross-section remains plane before and after bending; (2) valid bonding between concrete and prestressing tendons, steel bars and shaped steel is available; (3) failure in bending occurs before that in shearing for components of model, such as beams and columns; (4) shrinkage and creep in concrete and failure of panel zone are neglected.

3.1 Influence of prestressing

An principle of two stages for prestressing members is presented by Zheng [12] as follows: in the first stage, the forces at the beam end and the equivalent distributed load between joints are considered as external loads when effective prestressing stress is built by tensioning the prestressing tendons; in the second stage, the redundant strength exceeded the effective prestressing stress of tendons is used to resist the additional loads, thus the tendons could be thought as a certain type of material named as *prestressing tendons at second stage*. Therefore, the prestressed frame could be transformed into ordinary frame of two stages to carry the equivalent loads and service loads respectively, and then the loads of two stages could be superposed, as shown in Figure 16. Where N_p and M_p is the equivalent concentrated force and moment, respectively; the q_1 and q_2 is the equivalent distributed loads; N_1 and N_2 is the vertical concentrated loads applied on the top columns and beam respectively. The constitutive relationship of *prestressing tendons at second stage* could be obtained by moving the origin to the point of effective prestressing stress in the primary stress-strain curve of tendons, shown in Figure 20.
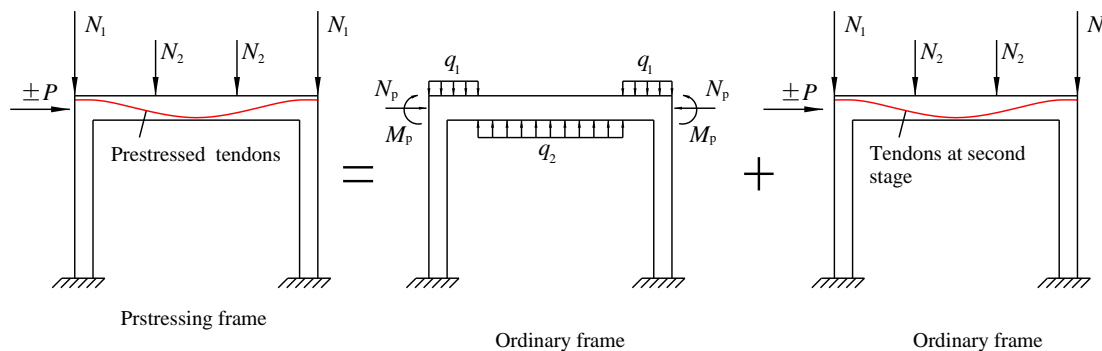

Fig. 16 Prestressed frame transformed into non-prestressed frame

3.2 Calculation model

The two specimens of single-story and single-span frame could be divided into beam-column elements with element nodes setting in the position of potential plastic hinges and cross-section changing of components. Figure 17 shows the elements and nodes distribution and cross-section division of the two specimens. In the modeling, the

fiber beam-column elements considering the plastic distribution (Nonlinear Beam Column Element) is adopted for the beam and columns of SRCF specimens and the columns of PSRCF specimens. While the fiber beam-column elements with concentrated plastic hinges (Beam with Hinges Element) are adopted for the beam of PSRCF due to the different cross-section along the beam axis.
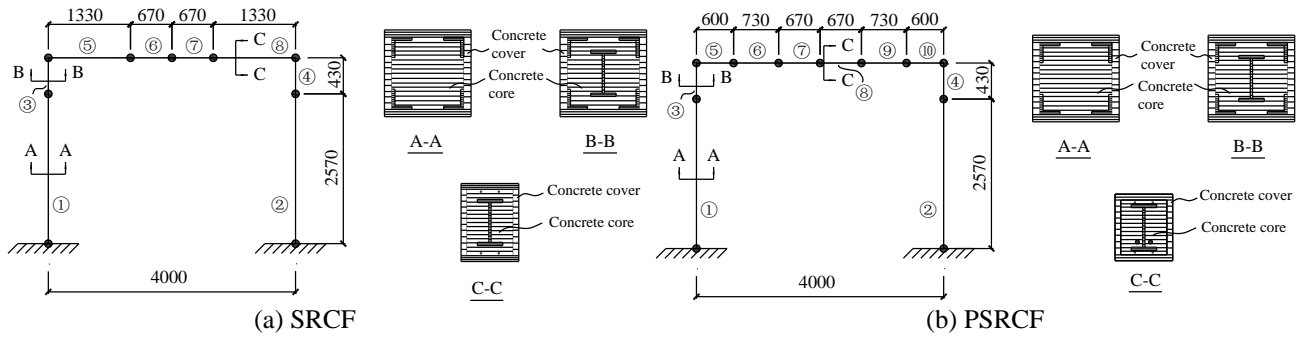
(a) SRCF   (b) PSRCF

Fig. 17 Analytic model for test specimens

3.3 Material constitutive relationship

Kent-Scott-Park model made up of ascending parabola and descent straight line under compression with degraded linear unloading/reloading stiffness proposed by Karsan and Jirsa [13] is adopted as concrete compressive stress-strain relation as shown in Figure 18, where f_c and Kf_c is the unconfined and confined concrete compressive strength respectively, ε_0 is the strain correspond to the confined concrete strength, Z_1 and Z_2 is the confined and unconfined concrete descent stage slope respectively. Unconfined and confined concrete model are accepted in the cover and core of cross-section of members respectively. In order to simplify analysis, steel plate hoops are equivalent to the stirrups based on the same areas, and the tensile strength of concrete [14,15] and the influence of I-shaped steel on concrete are neglected.
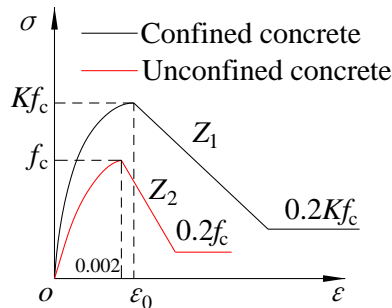

Fig. 18 Stress-strain relation for confined and unconfined concrete under compression

Bilinear kinematic model considering the Bauschinger effect shown in Figure 19 are utilized in angle-steel, steel plate hoop, I-shaped steel and steel rebars, which takes strengthening phase stiffness of $0.01E_s$.
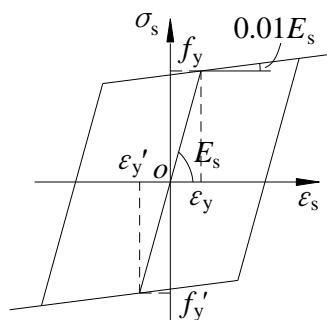

Fig. 19 Stress-strain relation of steel

According to the principle of the two stages for prestressing members, stress-strain relation for prestressing tendons at the second stage is shown in Figure 20, where $f_{p0.2}$ is the nominal yielding strength with the residential strain of 0.2% In this constitutive relation, skeleton curves include elastic and yielding regions, and the unloading and reloading go along straight line with elastic modulus of initial value. Meanwhile, the routing of reloading cannot exceed the skeleton curves.
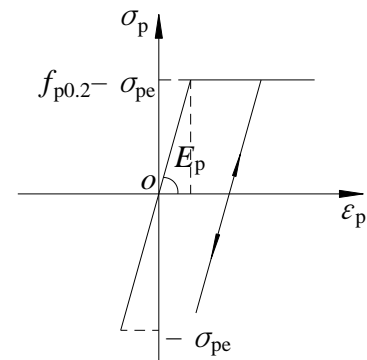

Fig. 20 Stress-strain relationship of prestressing tendons at second stage

3.4 Comparison of calculations and tests

The comparison of the ultimate bearing capacity, stiffness degradation and hysteretic curve shapes acquired by the tests with the calculation from OpenSEES in this paper are shown in Figure 21. They are basically in agreement with each other, while some differences are as follows:

(1) The skeleton curves from tests are a little smaller than calculation. The reason led to this reduction might be that no lateral supports are adopted in this test, as well as slenderness of columns could result in out-of-plane offset.

(2) There are some distinctions in softening segment of hysteretic loops between calculation and tests. The reason might be that bilinear kinematic model is accepted in steel without transitional arc in softening segment.

(3) The steel plate hoops are treated as equivalent area stirrups and the confined effect of encased steel on concrete is also not taken into account. These all may lead to the differences.

Overall, the employment of OpenSEES could meet the engineering requirements, and it could be used for the following parameter analysis.
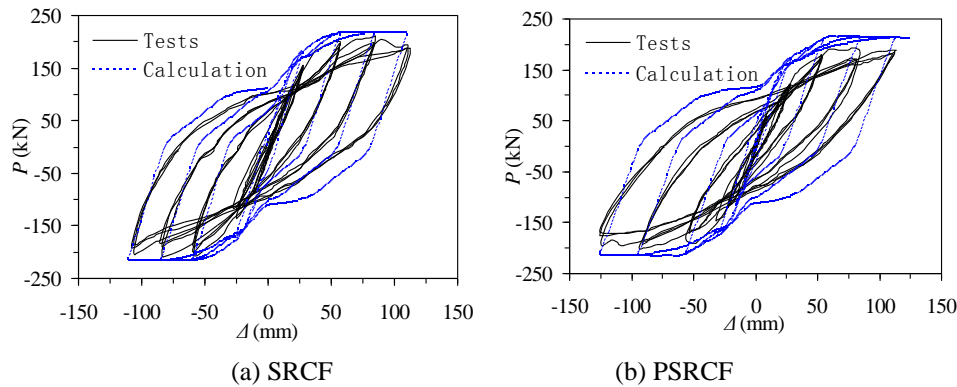
(a) SRCF   (b) PSRCF

Fig. 21 Comparison of hysteretic curves for specimens obtained from test and calculation

4. Parameter Analyses

For the further study of the seismic performance of SRCB-ASCC Frame, the slenderness ratio β, axial compression ratio n_0, steel ratio of column ρ_a, cross-section moment resistance of I-shaped steel W_{ss}, ratio of rebars of beam ρ_s and prestressing level λ are observed. Here prestressing level λ could be derived as follows approximately:

$$\lambda = \frac{A_p f_{p0.2} h_p}{A_p f_{p0.2} h_p + A_{ss} f_{ss} h_{ss} + A_s f_y h_s} \tag{1}$$

Where A_p, A_{ss} and A_s is the area of prestressing tendons, I-shaped steel flange and longitudinal rebars in the tension zone, respectively; $f_{p0.2}$、 f_{ss} and f_y is the yield strength of prestressing tendons, I-shaped steel flange and longitudinal rebars, respectively; h_p、 h_{ss} and h_s is the distance between concrete edge under pressure and centroid of the prestressing tendons, I-shaped steel flange and longitudinal rebars in the tension zone, respectively.

General conditions are given as follows: Concrete column section is 300mm×300mm with four angle-steels arranged at the corner symmetrically; Steel reinforced concrete beam section is 200mm×270mm with the span of 4000mm, where I-shaped steel and longitudinal rebars are decorated symmetrically. Prestressed steel reinforced concrete beam section is 200mm×230mm with the span of

4000mm, where I-shaped steel and longitudinal bars are also placed symmetrically. Vertical loads are only applied on the top of the columns due to the loads applied on the beam have minor influence on the hysteretic loops . From the results, the seismic performances of the prestressed and ordinary frames are close to each other, so this paper gives the results of prestressed frame only.

Figure 22 shows the influence of slenderness ratio β on P-Δ curves. As slenderness ratio β increase, ultimate load of P-Δ curves decrease with smooth descent segment and increasing displacement corresponding to ultimate load.

The influence of axial compression ratio n_0 on P-Δ curve is given in Figure 23. With axial compression ratio n_0 increasing, the ultimate load of P-Δ curves increases at first then fall off. Meanwhile the displacement corresponding to ultimate load decreases with abrupt descent segment and little ductility.

Along with the increasing of angle-steel ratio ρ_a in columns, cross-section moment resistance of I-shaped steel W_{ss} and longitudinal rebars ratio ρ_s in beam shown in Figure 24 and Figure 25, initial stiffness and ultimate load of P-Δ curves increase accompanied with similar slope of descent segment and semblable shape of P-Δ curves.

Figure 26 gives the influence of prestressing level λ on P-Δ curves. It indicated that the initial stiffness and horizontal carrying capacities of frames increase slightly with increasing prestressing level λ, and the reason could be due to the effect of I-shaped steel encased in beam.
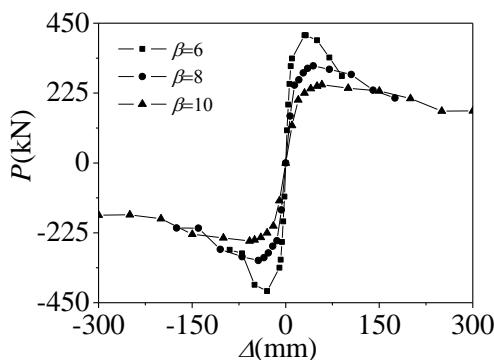

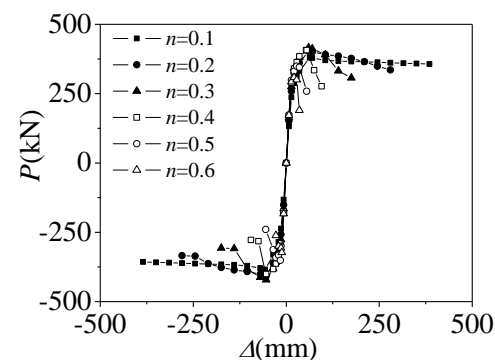**Fig. 22** influence of β on P-Δ curves
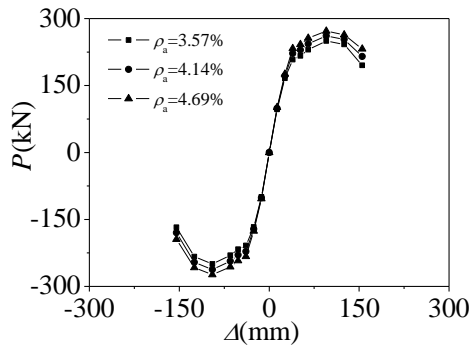

Fig. 23 influence of n_0 on P-Δ curves

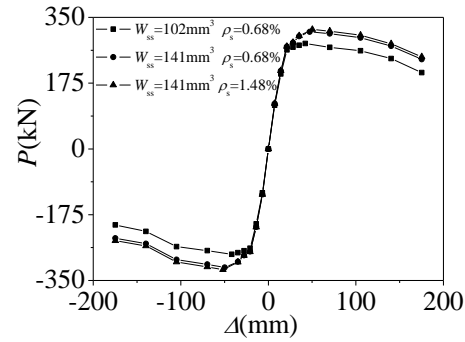**Fig. 24** influence of ρ_a on P-$\varDelta$ curves

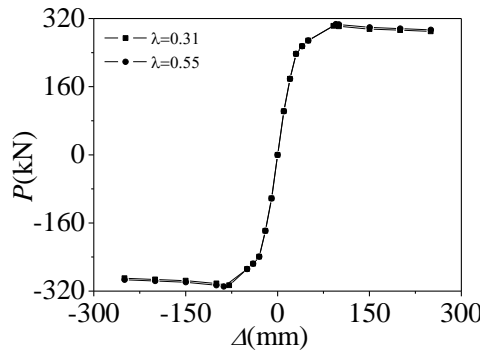**Fig. 25** influence of W_{ss} and ρ_s on P-$\varDelta$ curves

Fig. 26 influence of λ on P-$\varDelta$ curves

5. Comparisons with Other Frames

Equivalent adhesive damper coefficient ξ_{eq} is usually used to assess the seismic performance of frames. Table 4 lists the calculated equivalent adhesive damper coefficient under different types of frames from tests of Li [16] and Fu et al [9]. It is observed that the energy dissipation of frame structure of steel reinforced concrete beam and angle-steel concrete column is similar to that of steel reinforced concrete members with solid-web, and is better than prestressed reinforced concrete frame.

Table4 Equivalent adhesive damper coefficient under different type of frame

Type of Frame	ξ_{eq}
Prestressed reinforced concrete frame	0.15
Prestressed reinforced concrete frame (with solid-web members)	0.18
Steel reinforced concrete frame (with solid-web members)	0.20
Prestressed frame of steel reinforced concrete beam and angle-steel concrete column	0.19
Frame of steel reinforced concrete beam and angle-steel concrete column	0.20

6. Recommendation of Collapse-Resisting

The collapse of the soft storey mechanism could occur in the ground floor due to the higher columns, which could be several times length of the ordinary ones. Thus, in order to prevent from this type of failure mechanism, there are two ways to increase the capacities of ground floor columns to postpone the occurring of the plastic hinges at

the column ends: (1) enhance the seismic grade of the columns in the ground floor according to the Chinese code; (2) amplify the ratio of strong-column weak-beam.

7. Conclusions

This paper describes experimental and numerical investigations on two frame structures of steel reinforced concrete beam and angle-steel concrete column under horizontal low cyclic loading, the primary results are summarized as follows:

(1) A new type of out-jacketing frame structure composed of steel reinforced concrete beam and angle-steel concrete column (SRCB-ASCC Frame) for adding storeys around existing building based on the idea of self-weight-carried floor under construction is developed, which has an advantage over the conventional ones as the steel beam can carry the self weight of the frame beam and the construction loads when the frame is under construction, and the steel reinforced concrete beam and the angle-steel concrete column could work as a unit to carry remainder loads in the serviceability stage.

(2) From the test results, the hysteretic loops of the two specimens of SRCB-ASCC Frame are relatively plump and have the spindle shape, and it indicated that the two specimens have good energy dissipation capacities; The secant stiffness of two specimens reduces gradually with the increasing of displacement and the stiffness degradation curves are closed to each other, it is found that the prestressing has little effect on the stiffness degradation; It is also found that prestressed test specimen has better deformation restoring capacities since its residual deformation is less than that of the nonprestressed one except for $\varDelta \approx 27mm$. Moreover, the frame beam depth

K. Wang, S.F. Yuan, D.F. Cao, W.Z. Zheng

is reduced from 230mm to 270mm when prestressed, and it illustrated that the prestressing could decrease the frame beam depth to improve the service function.

(3) The nonlinear structural analysis program OpenSEES is employed to calculate the hysteretic loops, and the comparison of the calculations with the tests on the ultimate bearing capacity, stiffness degradation and hysteretic curve shapes are acquired. The results of calculations and tests are basically in agreement with each other. So, it could be used for the consequent parameter analysis.

(4) From the numerical analysis results, with slenderness ratio of column increasing, ultimate load of P-Δ curves decrease, the displacement corresponding to ultimate load increase and the descent segment becomes smooth; With axial compression ratio increasing, ultimate load of P-Δ curves increase at first then fall off, the displacement corresponding to ultimate load increase and the descent stage is steeper; With angle-steel ratio of column, cross-section moment resistance of I-shaped steel, longitudinal rebars ratio in beam, and prestressing level increasing, the initial rigidity, ultimate load and the displacement corresponding to ultimate load of P-Δ curves increase in different degree.

(5) It is observed from the tests that the equivalent adhesive damper coefficients of the two specimens of SRCB-ASCC Frame are 0.20 and 0.19 respectively, which are close to that of steel reinforced concrete frames with solid-web members and bigger than that of prestressed reinforced concrete frame. And it indicated that the hysteretic behaviors of SRCB-ASCC Frame and steel reinforced concrete frame with solid-web members are similar to each other and better than prestressed reinforced concrete frame.

References

[1] Zheng WZ, Sun XJ. Methods and practice on adding storeys around existing buildings, Concrete Engineering International, 2008, No. 3, Vol. 12, pp. 62-63.

[2] Sun XJ, Cao JP, Zheng WZ. Seismic elastic-plastic analysis on outer-jacketing mega frame for story-adding by IDARC-2D, Advanced Materials Research, 2011, pp. 255-260, pp. 209-214.

[3] Zheng WZ, Wang K, Zhang GM. Experimental study on hysteretic behavior of prestressed truss concrete composite beams, Earthquake Engineering and Engineering Vibration, 2010, No. 1, Vol. 9, pp. 65-74.

[4] Zhao HT. Steel & Concrete Composite Structure, Science Press, Beijing, 2001, in Chinese.

[5] Zheng WZ, Ji J. Dynamic performance of angle-steel concrete columns under cyclic loading-I: Experimental study, Earthquake Engineering and Engineering Vibration, 2008, No. 1, Vol. 7, pp. 67-75.

[6] Zheng WZ, Ji J. Dynamic performance of angle-steel concrete columns under cyclic loading-II: Parametric study, Earthquake Engineering and Engineering Vibration, 2008, No. 1, Vol. 7, pp. 137-146.

[7] Xue WC, Yang F, Su XL, Lu P. Experimental studies on prestressed steel reinforced concrete beams under low reversed cyclic loading, Journal of Harbin Institute of Technology, 2007, No. 8, Vol. 39, pp. 1187-1190. in Chinese.

[8] Zhao GD, Fu CG, Lu XL. Experimental study on the rigidity behavior of prestressed steel reinforced concrete beams, Electric Technology and Civil Engineering, International Conference, 2011, pp. 2240-2243.

[9] Fu CG, Li YY, Sun XB, Xu J. Experimental study on seismic performance of prestressed and non-prestressed steel reinforced concrete frames, Journal of Building Structures, 2010, No. 8, Vol. 31, pp. 15-21, in Chinese.

[10] Wang K, Luo HH, Zheng WZ. Performance of frame structure composed of steel reinforced concrete beam and angle-steel concrete column under horizontal loading, Applied Mechanics and Materials, 2012, Vol. 204-208, pp. 1094-1101.

[11] Mazzoni S, Mckenna F, Scott MH, Fenves GL, Jeremic B. OpenSEES Command Language Manual, Berkeley, 2003.

[12] Zheng WZ, Wang Y. Uniform design method and examples for prestressed concrete building structures, Heilongjiang Science and Technology Press, Harbin, 1998, in Chinese.

[13] Karsan ID, Jirsa JO. Behavior of Concrete under Compressive Loading, Journal of Structural Division, ASCE, 1969, Vol. 95, pp. 2543-2563.

[14] Kent DC, Park R. Flexural members with confined concrete, Journal of the Structural Division, ASCE, 1971, No. 8, Vol. 97, pp. 1969-1990.

[15] Scott BD, Park R, Priestley MJN. Stress-strain behavior of concrete confined by overlapping hoops at low and high strain rates, ACI Journal, 1982, No. 1, Vol. 79, pp. 13-27.

[16] Li ZQ. Research on the seismic behaviors of prestressed concrete frame, Ph D thesis, Chongqing University, Chongqing, 2006, in Chinese.